

# Engineering Cell Surface Function with DNA Origami

Ehsan Akbari, Molly Y. Mollica, Christopher R. Lucas, Sarah M. Bushman, Randy A. Patton, Melika Shahhosseini, Jonathan W. Song,\* and Carlos E. Castro\*

**A specific and reversible method is reported to engineer cell-membrane function by embedding DNA-origami nanodevices onto the cell surface. Robust membrane functionalization across epithelial, mesenchymal, and non-adherent immune cells is achieved with DNA nanoplatforms that enable functions including the construction of higher-order DNA assemblies at the cell surface and programed cell–cell adhesion between homotypic and heterotypic cells via sequence-specific DNA hybridization. It is anticipated that integration of DNA-origami nanodevices can transform the cell membrane into an engineered material that can mimic, manipulate, and measure biophysical and biochemical function within the plasma membrane of living cells.**

The cell plasma membrane is the primary mediator of communication between the cell and its surrounding environment. The ability to monitor or synthetically control the cell membrane is an attractive approach to engineer the function of cells or their local microenvironment. One approach to manipulate cell membrane function is by exploiting cell machinery to modify existing membrane proteins or express novel recombinant gene products on the cell surface.<sup>[1]</sup> However, this approach is generally limited to modifying membrane proteins instead of introducing nonnative functions with the possibility of external control or measurable readouts. Recent advances in biomolecular engineering have also enabled installing new functions into cell membranes via external integration of compounds

expand capabilities to engineer cell membranes as a programmable and responsive material.

Structural DNA nanotechnology,<sup>[8]</sup> specifically the molecular self-assembly process known as DNA origami,<sup>[9]</sup> has emerged as a versatile approach to fabricate nanodevices with complex nanoscale geometry, defined placement of molecular functionalities, and programed mechanical and dynamic properties. DNA origami devices have wide-ranging applications, including drug delivery,<sup>[10–12]</sup> sensing,<sup>[13,14]</sup> molecular manipulation,<sup>[15]</sup> and measurement.<sup>[16,17]</sup> Hence, robust methods to incorporate DNA origami devices onto cell membranes could enable straightforward access to a variety of functions to probe and control cell behavior. Prior work attaching DNA origami structures to synthetic lipid bilayers has been conducted for a variety of purposes as reviewed recently<sup>[18]</sup> such as the construction of synthetic nanopores for ion and molecular transport,<sup>[19,20]</sup> examination of membrane diffusion and ordering characteristics,<sup>[21,22]</sup> and directed assembly of nanostructure arrays.<sup>[23]</sup> In addition, recent work has also used DNA nanostructures to template the shape of lipid assemblies.<sup>[24]</sup> However, these studies are limited to synthetic bilayers, which lack the structural complexity of live cell membranes. Other recent work has leveraged the ability to template ligands on DNA origami structures to study cell signaling;<sup>[25]</sup> however, these studies rely on binding to a specific surface receptor and hence are not easily translatable to many cell types.


Here, we establish a foundation for implementing the diverse function of DNA origami nanotechnology on cell surfaces by using hydrophobic anchors to attach 3D DNA origami nanostructures to the surface of five distinct cell types, including adherent, suspension, and primary cells. Our method uses cholesterol-conjugated oligonucleotides as amphiphilic anchors that incorporate into the plasma membrane to facilitate installation of DNA origami structures onto the surface of living cells. This method is specific, reproducible, and reversible. We demonstrate installation of a DNA nanoplatform that functions as a molecular-scale membrane-bound breadboard

E. Akbari, M. Y. Mollica, Dr. C. R. Lucas, R. A. Patton, M. Shahhosseini  
Department of Mechanical and Aerospace Engineering  
The Ohio State University  
Columbus, OH 43210, USA

S. M. Bushman  
Department of Biomedical Engineering  
The Ohio State University  
Columbus, OH 43210, USA

Prof. J. W. Song  
Department of Mechanical and Aerospace Engineering  
The Ohio State University Comprehensive Cancer Center  
The Ohio State University  
Columbus, OH 43210, USA  
E-mail: song.1069@osu.edu

Prof. C. E. Castro  
Department of Mechanical and Aerospace Engineering  
Biophysics Graduate Program  
The Ohio State University  
Columbus, OH 43210, USA  
E-mail: castro.39@osu.edu

 The ORCID identification number(s) for the author(s) of this article can be found under <https://doi.org/10.1002/adma.201703632>.

DOI: 10.1002/adma.201703632

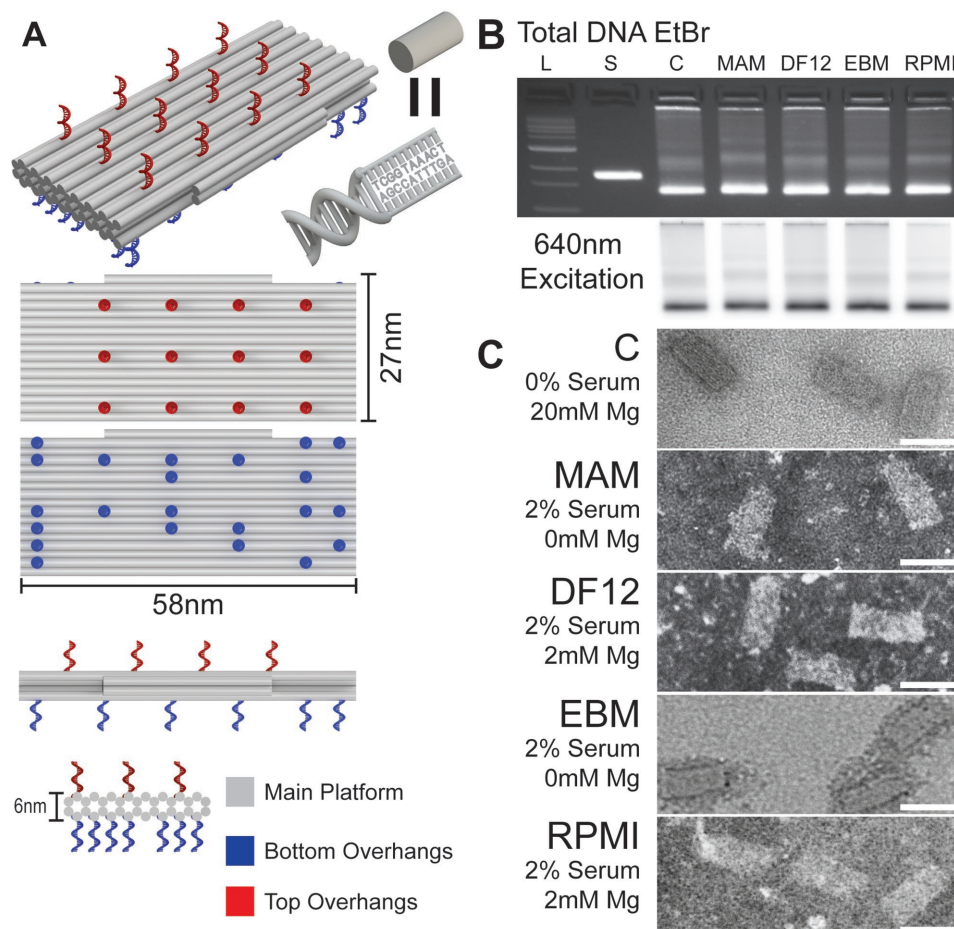


**Figure 1.** Design and characterization of the MBB. A) Isometric, top, bottom, and side views illustrate the structure design and locations of the top (red) and bottom (blue) overhangs. Gray cylinders represent dsDNA helices. B) Gel analysis confirms MBB structural stability after 3 h in each cell-specific media and cell culture conditions (37 °C, 5% CO<sub>2</sub>). Total DNA and the fluorescently labeled overhangs were visualized with UV excitation (top) and 640 nm excitation (bottom), respectively. The DNA scaffold is S, the control structure in folding buffer is C, and the remaining four lanes illustrate results after incubation in the four cell-culture conditions. C) TEM images confirm the structure of the MBB is preserved after incubation under cell culture conditions for 3 h in storage buffer (top) and the four cell media conditions. Scale bars are 50 nm. Both (B) and (C) are representative images from three independent experiments.

(MBB) that can be programmed with multiple functions such as sequence-specific binding or fluorophores at defined locations. The sequence-specific binding allows the MBB to be used as a docking site for controlled spatial positioning of additional DNA-based constructs, devices, or higher order assemblies on the cell surface. We demonstrate this capability by programming both homotypic and heterotypic cell–cell binding where the sequence-specific DNA base pairing between MBBs on adjacent cells serves as a cellular Velcro (or “CellCro”). We envision that multifunctional DNA origami devices can transform the cell membrane into a programmable material that exploits the broad scope of biomolecular nanotechnology.

The MBB (≈58 nm × 27 nm × 6 nm) consists of 34 double-stranded DNA (dsDNA) helices organized into two layers on a honeycomb lattice<sup>[26]</sup> (Figure 1A; Figure S1 and Table S1, Supporting Information). It is designed to enable the selective incorporation of up to 34 single-stranded DNA (ssDNA) overhangs (up to 12 overhangs on the outward-facing side and up to 22 on the cell-facing side) in which select strands extend out

of the structure by 20 bases (Figure 1A; Figure S1, Supporting Information).

Previous work demonstrated that the structural integrity of DNA origami nanostructures is sensitive to the concentration of cations and the presence of nucleases in cell culture media.<sup>[27]</sup> Therefore, we tested the stability of the MBB in the media conditions required for each cell type of interest. In this study, the overhangs are essential to anchor the structure to the membrane and as sites for programming binding or fluorophore readouts. To quantify the stability of the overhangs, they were labeled with a complementary strand conjugated to an Alexa 647 fluorophore. The structures were incubated in each cell culture media or control buffer for 3 h, which covers our experiment timescale, and the MBB stability was analyzed via agarose gel electrophoresis with ethidium bromide staining to monitor the structure and fluorescent gel imaging to monitor the overhangs. We observed no significant degradation of the platform structure or overhangs under each selected cell culture media conditions compared to the corresponding control structures

in folding buffer (Figure 1B). To extend these findings, MBBs were then extracted from the gel and visualized via transmission electron microscopy (TEM), which confirmed that MBBs preserved their structural integrity (Figure 1C). Together, these findings show that the MBB is stable in a range of cell culture media conditions containing 2% serum and 0–2 mM MgCl<sub>2</sub>, which enables its use with a large variety of cell types. A similar approach was used to examine MBB stability over 24 h in similar cell culture media conditions for cell types of interest over a range of serum levels and MgCl<sub>2</sub> concentrations. After 24 h, both MBB and overhang stability improved with lower serum levels and higher levels of MgCl<sub>2</sub> (Figure S2, Supporting Information), which is consistent with previous stability studies.<sup>[27,28]</sup> Quantitative analysis of the gel band intensity showed that after 24 h, overhangs are increasingly lost from the MBB with serum levels >2% (Figure S2 and S3, Supporting Information). In addition, overhangs are lost from MBBs after 24 h at MgCl<sub>2</sub> concentrations ≤1 mM MgCl<sub>2</sub> (Figure S2 and S3, Supporting Information). Interestingly, different media yielded different stabilities of structures and overhangs, with DF12 providing the most robust stability up to 10% serum and down to 0 mM MgCl<sub>2</sub>. Since overhangs proved to be the limiting stability, we selected cell culture media conditions that yielded stable overhangs up to 24 h (Figure 1C).

To enable a specific, controllable, and reversible scheme to attach DNA origami nanostructures to living cell membranes, we chose to first functionalize cells with DNA strands to exploit the specificity of DNA base pairing. This enables binding of nanostructures only to cells functionalized with the appropriate DNA strands. We implemented cholesterol-conjugated oligonucleotides to attach an ssDNA strand to the membrane by incorporation of the hydrophobic cholesterol moiety into the hydrophobic inner belt of a lipid bilayer anchoring the ssDNA oligonucleotides to which the MBB could subsequently bind (Figure 2A). Visualization of fluorescently labeled oligonucleotides complementary to the membrane-incorporated oligos (MIO) confirmed their successful insertion into the cell membrane (Figure S4, Supporting Information).

Instead of binding the MBB structure directly to the MIO, we utilized an intermediate 60-base oligonucleotide to bridge the MBB to cell membrane. The bridge oligo binds to the MIO via 20 complementary bases on one end and binds to MBB overhangs via 20 complementary bases at the opposite end. This bridge oligo provides two key advantages. First, it extends MBB binding sites from the cell surface to overcome the steric hindrance of the crowded cell membrane; and second, the middle section provides a site for strand displacement to remove the MBB from the cell surface. The bridge oligo was added to cells functionalized with the MIO, and in most experiments, a 20-base oligo complementary to the middle portion of the bridge was then added to mechanically fortify the bridge strand (Figure 2A). For later removal experiments, this fortifier strand was not included. After the successful addition of MIO, bridge oligos, and the bridge fortifier oligos, fluorescently labeled MBBs were added to the cell membrane (Figure 2A). In addition to the complete functionalization, three control conditions were included to confirm specificity: absence of the MBB (Control I) (Figure 2B,i), absence of the MIO (Control II) (Figure 2B,ii), and a case where the binding between the bridge oligo and the MIO was blocked

via a strand, referred to as the binding inhibitor oligo (BIO), that was added to the bridge to occupy the 20 bases that would normally bind to the MIO (Control III) (Figure 2B,iv).

We used the aforementioned binding scheme to functionalize the surface of five distinct cell types, including primary human pancreatic fibroblasts (HPF), and four cell lines: human breast epithelial cells (MCF-10A), human umbilical vascular endothelial cells (HUVEC), human promyelocytic leukemia cells (HL-60), and mouse lymphoma B cells (CH12.LX). MBBs were labeled with Alexa 647 and binding was visualized via epifluorescence microscopy (Figure 2C). Binding of MBBs to the membrane of each cell type was clear upon complete functionalization and was completely inhibited when binding between MIO and the bridge oligo was blocked, confirming the specificity of our scheme independent of the cell type. No significant binding was observed in the absence of the MIO (Control II). These results highlight the specificity of attaching the MBB to MIO at the cell surface. The fluorescence intensity attributed to MBBs on the surface of cells was measured using a custom MATLAB code and parameterized in terms of the mean fluorescence intensity around the perimeter of individual cells (Figure S5, Supporting Information). The mean fluorescence intensity for individual cells was normalized to the overall average of the mean fluorescence intensity under the corresponding Control I condition for that particular cell type. With the prescribed functionalization scheme, the mean fluorescence intensity from the MBB was significantly increased relative to all controls (Figure 2C). In the case of HUVECs, some minimal nonspecific binding of MBBs to the cell surface occurs, which is not blocked by the binding inhibitor oligo further confirming the significant amount of specific binding. To extend these findings, we obtained the 3D distribution of MBBs bound to the surface of a single CH12.LX cell surface via confocal microscopy (Figure S6, Supporting Information), which confirmed the uniform presence of structures on the cell surface. The consistent signal around the cell periphery cell also ruled out internalization of MBBs over the time course of the functionalization. The absence of significant binding to the cell surface in the absence of the MIO was also confirmed via confocal microscopy (Figure S6, Supporting Information). Taken together, these findings confirm that our functionalization scheme enables robust and specific attachment of MBBs to the surface of five distinct cell types.

To demonstrate DNA nanostructures as versatile tools within the context of the cell membrane, we developed two programmable features of the MBB that demonstrate real-time control over nanostructure assembly at the cell surface. We first illustrated controllable detachment of MBBs from a cell surface using DNA strand displacement,<sup>[29]</sup> which is widely used to reconfigure DNA nanostructures or to carry out logic steps in molecular computing.<sup>[30,31]</sup> For removal experiments, we excluded the bridge fortifier oligos to exploit the middle region of the bridge oligo as a site to nucleate binding and strand displacement using 40-base detachment oligos (Figure 3A). Incubation of the functionalized CH12.LX cells with detachment oligos resulted in significant reduction in MBBs attached to the cell surface (Figure 3B). Exponential fits to the fluorescence decay data revealed that ~90% of MBBs were removed after 1 h, with most removed within 15 min. To confirm that

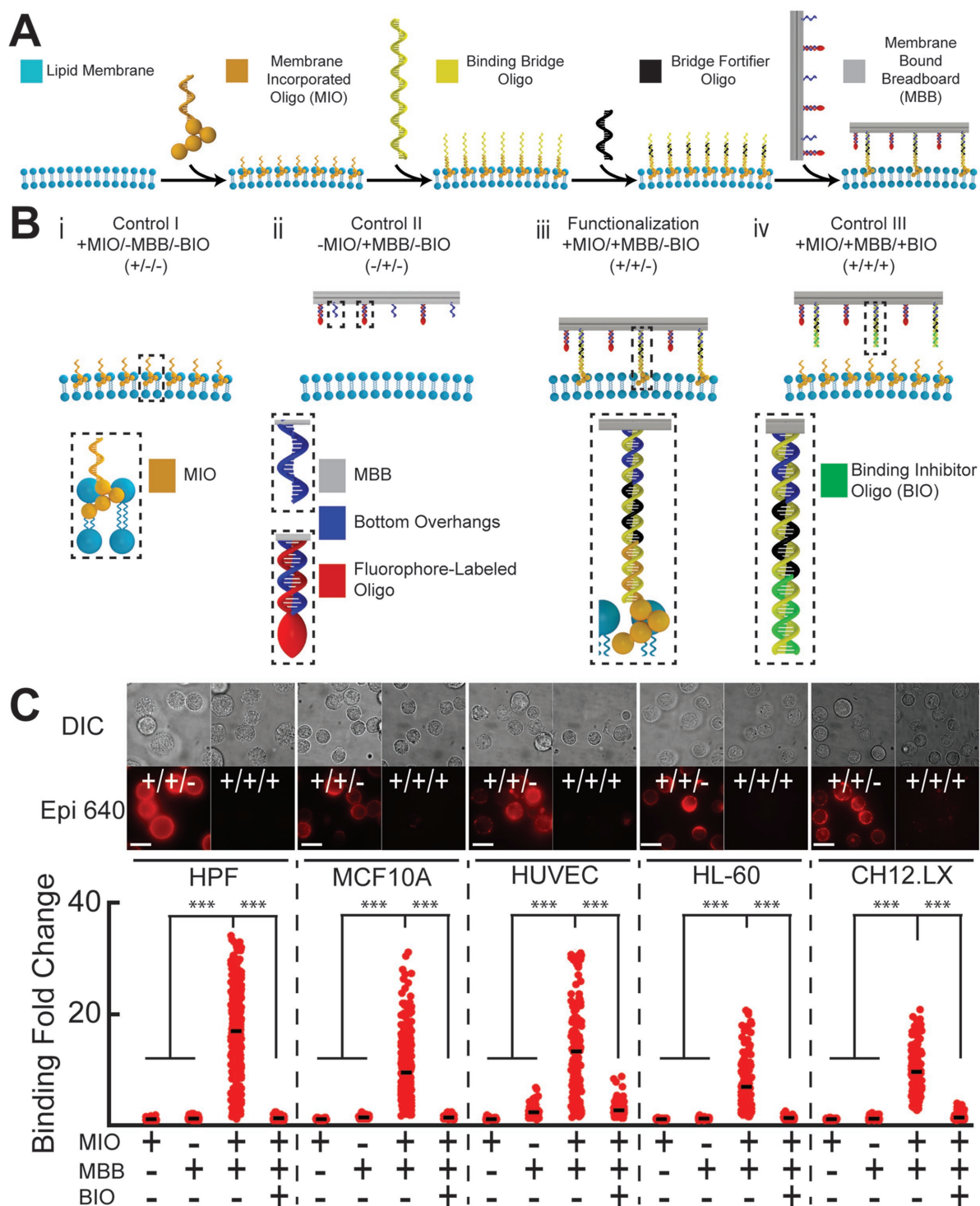


**Figure 2.** Scheme to functionalize the cell membrane with the MBB. A) The detailed illustration of the sequential functionalization steps includes integration of the MIO into the cell membrane followed by binding of bridge oligos and bridge fortifier oligos. The bridge oligo presents a base-pairing site for the specific binding of MBBs. B) Schematics of each experimental condition including: i) MIO only as experimental Control I; ii) Alexa-647-labeled MBBs introduced in the absence of the MIO as Control II; iii) the complete functionalization scheme including binding of Alexa 647-labeled MBBs; and iv) binding inhibited by a 20-base oligo that hybridizes to the MIO binding site of the bridge strand followed by introduction of Alexa 647-labeled MBBs as Control III. C) The aforementioned controls and the complete functionalization were carried out for five cell types including primary HPF and four cell lines—MCF10A, HUVEC, HL-60, and CH12.LX—followed by bright-field and fluorescence imaging (640 nm excitation). Representative images are shown from three independent experiments. Scale bars are 10  $\mu$ m. The mean fluorescence intensity attributed to the MBB bound to the surface of 100–300 single cells was quantified based on three independent experiments. The data are expressed as fold change in binding relative to the overall average of the mean fluorescence intensity quantified for Control I for each cell type. \*\*\*,  $p < 0.001$ .

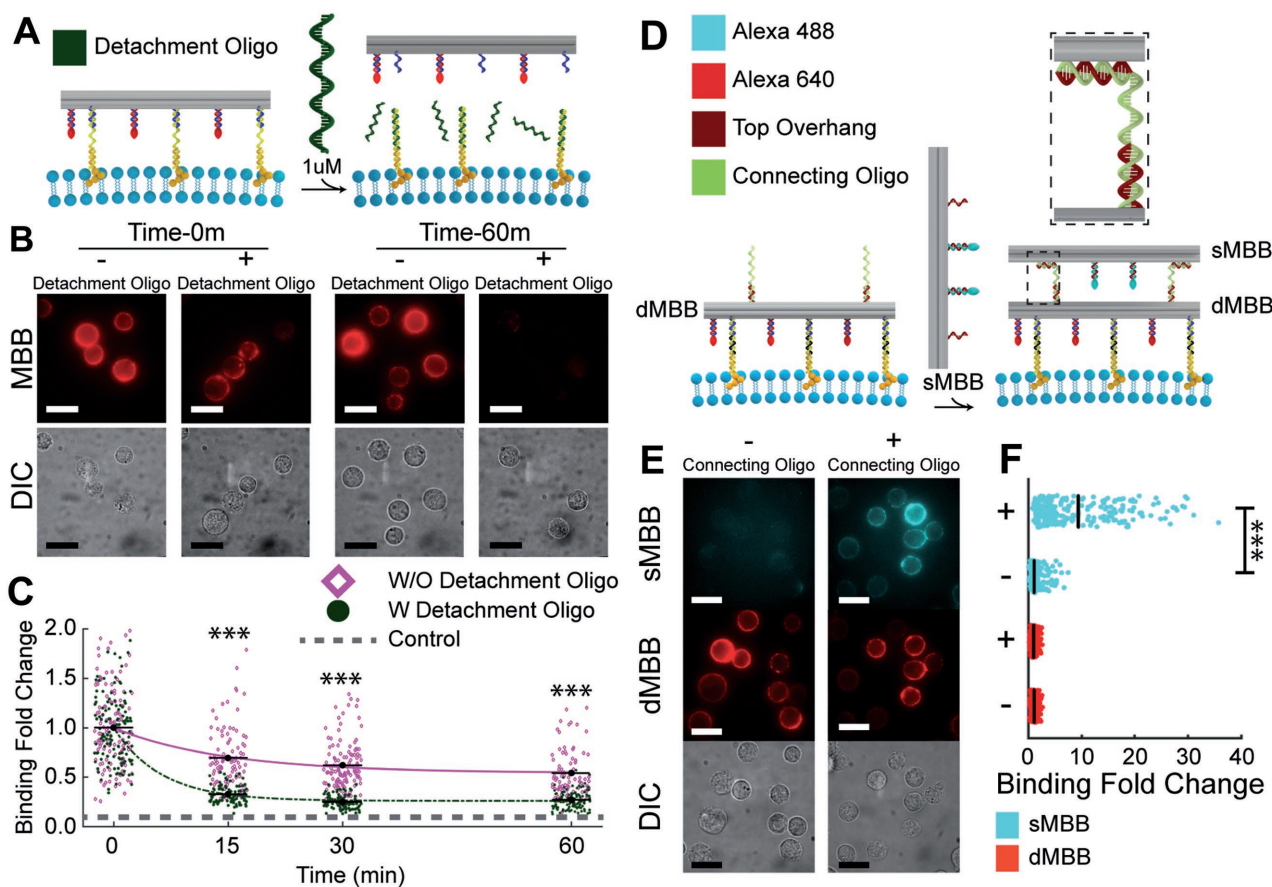


**Figure 3.** Detachment and hierarchical assembly of MBBs on the surface of CH12.LX cells. A) Strand displacement was utilized to remove the MBBs attached to the cell surface through the addition of detachment oligos. B) Qualitative assessments of MBB bound to CH12.LX with and without the addition of the detachment oligo. C) Quantification of the strand displacement-driven MBB detachment compared to the nonspecific reduction in the MBB fluorescence signal over time. D) The scheme for vertical dimerization of MBBs on the surface of CH12.LX cells includes initial attachment of Alexa 647-labeled dMBB, which featured COs on the outward-facing surface, followed by addition of a sMBB labeled with Alexa 488 fluorophores. E) Qualitative assessments of vertical dimerization on the cell surface. F) Quantification of vertical dimerization revealed an  $\approx 10$ -fold increase in binding of the sMBBs in the presence of the COs. Scale bars are 10  $\mu\text{m}$ . \*\*\*,  $p < 0.001$ .

this was not due to an inherent cellular mechanism removing MBBs from the cell surface, we also imaged MBBs on the cell surface at varying time points after functionalization in the absence of the displacement oligo revealing a relatively slow loss of MBBs on the cell surface with  $\approx 50\%$  of MBBs remaining after 1 h (Figure 3C). The level of MBB attached to the surface then remained steady up to 2 h, and we confirmed that the nonspecific decrease in the level MBB was not due to the absence of the fortifier oligo (Figure S7, Supporting Information). Internalization of the bound nanostructures was evident after 1 h based on epifluorescence time lapse images (Figure S7D, Supporting Information), suggesting that the nonspecific decrease in the level of bound MBB is likely due to the internalization of a fraction of the nanostructures after functionalization. Overall, these results confirm the capability to controllably detach MBBs from the cell surface.

A key goal of this work was to establish the MBB as a tool to dock additional devices onto the cell surface. We demonstrate this concept by docking an additional DNA origami platform nanostructure on the top of the MBB. For this purpose, the outward-facing side of MBBs was equipped with 12 binding

overhangs designed to enable hybridization-mediated docking of a secondary platform structure via 45-base connecting oligos (COs) (Figure 3D). Initial attachment of Alexa 647-labeled docking MBBs (dMBB), which included 12 overhangs on the outward-facing side prehybridized to COs, to CH12.LX cell membranes was carried out as previously described with comparable levels of binding (Figure 3E). The dMBB-functionalized cells were then incubated with secondary MBB (sMBB) structures labeled with Alexa 488 that were programmed to bind to the dMBBs. sMBBs exhibited significant binding to the cell surface (Figure 3E). We confirmed that binding between the sMBB and dMBB required the CO (Figure 3E,F). These findings illustrate that the MBB may serve as a foundation for higher order assemblies and a general docking site for DNA origami structures on the cell surface.

To demonstrate a functional application of the MBB, we leveraged the programmable assembly of complementary MBBs on the cell surface to facilitate controllable attachment between two cells. For this purpose, we designed MBB structures containing 22 binding overhangs on the cell-facing surface and 12 overhangs on the outward-facing surface (Figure 4A). Six overhangs

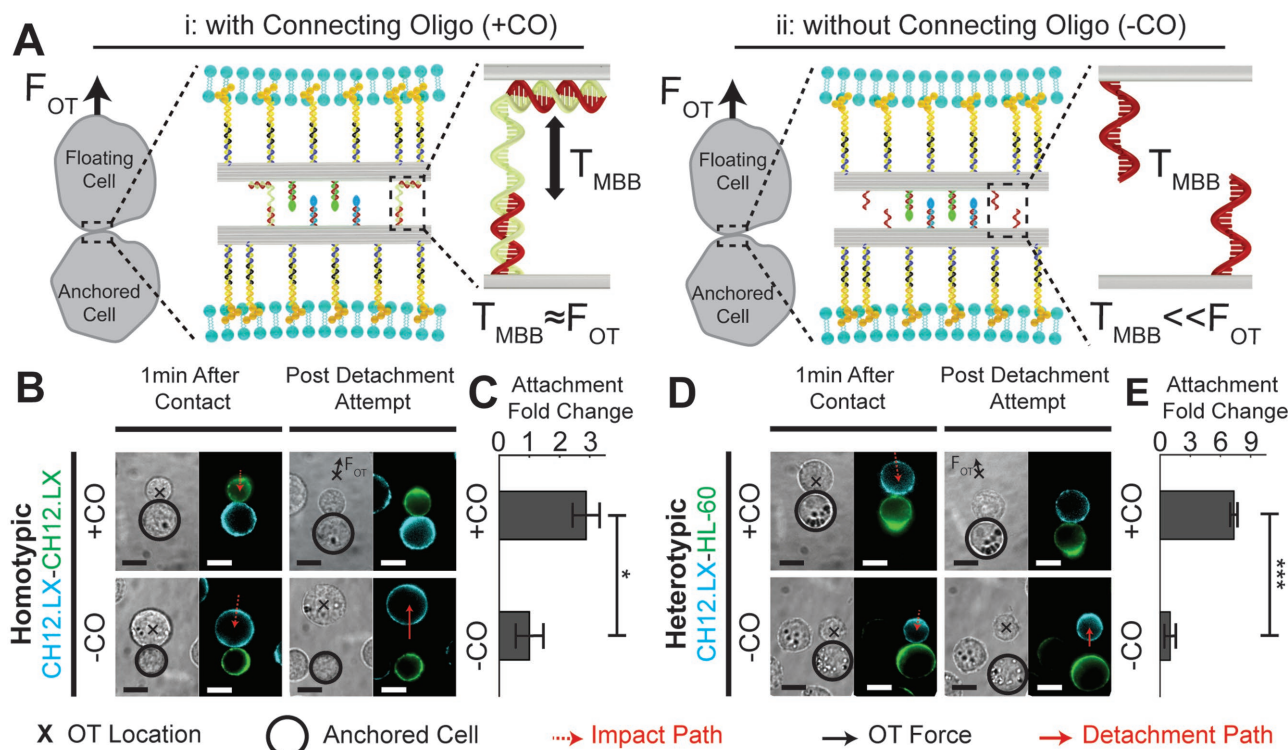


**Figure 4.** The MBB enables programmed adhesion between two living cells. A) Schematic of the i) intercellular adhesion facilitated by binding between dMBB and sMBB structures bound to distinct cells via hybridization of the CO. ii) In the absence of CO, binding between the two cells is not expected.  $F_{OT}$  and  $T_{MBB}$  refer to the force generated by the optical trap and the total tension supported by MBB binding interactions, respectively. Representative differential interference contrast (DIC) and fluorescence images showing MBB-mediated adhesion between functionalized B) CH12.LX to CH12.LX cells and D) CH12.LX to HL-60 cells. An optical trap (black cross in DIC images) was used to manipulate a floating cell toward a cell anchored to the surface (dashed black circle in DIC image). Cell–cell contact was maintained for  $\approx 1$  min. After incubation, the optical trap was used to apply tension at the cell–cell interface by steering the floating cell away from the anchored cell. The inability to dissociate the two cells was used as an indicator for successful attachment between the two cells. Quantification of the fraction of successful attachments between C) CH12.LX to CH12.LX cells and E) CH12.LX to HL-60 cells normalized with respect to the control condition in the absence of CO. Each condition was tested by three independent experiments and each repeat includes ten independent measurements. \*,  $p < 0.05$ . \*\*\*,  $p < 0.001$ . Error bars depict the standard error of the mean. Scale bars are 10  $\mu$ m.

on the outward-facing side of the MBB were designated as locations to program complementary cell binding. One set of cells was labeled with dMBBs where these six sites contained the CO overhang. A second set of cells was labeled with sMBBs where six overhangs were programmed to be complementary to the dMBBs. The remaining overhangs on the outward-facing surface were used to fluorescently label the dMBB and sMBB with Alexa 488- and Cy3-conjugated oligos, respectively.

The dMBB-labeled and sMBB-labeled cells were mixed in media and introduced into an imaging chamber under conditions that resulted in some cells anchored to the bottom surface of the chamber and some floating in media. Specific connections between an anchored dMBB-labeled cell and a floating sMBB-labeled cell, or vice-versa, were engaged by manipulating the floating cell with an optical trap (Movie S1 and S2, Supporting Information). Cells were held in contact for 1 min, and the MBB-mediated cell–cell attachment was then evaluated by applying tension on the dMBB–sMBB connection at the cell–cell junction with the optical trap (Movie S3 and S4, Supporting Information). The fraction of cell–cell adhesions that were not disrupted by the optical trap was used as an indicator of mechanically stable attachment mediated by dMBB–sMBB binding. The dMBB–sMBB attachment mediated by the CO

provided increased stability against tension compared to the control condition in the absence of CO (Figure 4A).

To evaluate the versatility of programming cell–cell binding, we tested two different scenarios: homotypic and heterotypic cell–cell interactions. The homotypic attachment, where both sets of labeled cells (dMBB and sMBB) were CH12.LX (Figure 4B), resulted in an  $\approx 3$ -fold increase in the fraction of mechanically stable cell–cell adhesions compared with the condition without CO (Figure 4C). In the heterotypic cell–cell attachment, we tested the adhesion between CH12.LX and HL-60 cells (Figure 4D). In the presence of CO, we observed an  $\approx 7$ -fold increase in the fraction of mechanically stable cell–cell adhesions between CH12.LX and HL-60 cells compared to the absence of CO (Figure 4E). These results confirm that programmed MBB binding enables controlled cell–cell adhesion for both homotypic and heterotypic interactions.

Previous studies implemented DNA devices in artificial lipid bilayers to study membrane diffusion, nanopore translocation, ordering transitions, and to control nanostructure actuation.<sup>[19,21,22,32]</sup> To enable these and many other functions of DNA nanodevices at the cell surface, we developed a technology for specific and controllable attachment of DNA origami nanodevices to the membrane surface of multiple cell types.

Our anchoring approach utilized cholesterol-conjugated oligos as DNA–lipid hybrids, as done in previous reports.<sup>[19,21]</sup> Here, we demonstrated the ability of the chemically modified oligos to serve as amphiphilic anchors into the plasma membrane of living cells. A key feature of our live cell functionalization approach is the use of additional oligo to extend ssDNA binding sites above the surface to overcome steric hindrance to binding near the cell surface. The successful functionalization of a range of cells, including primary human fibroblasts, adherent cell lines, and suspension cell lines illustrates the robustness of this approach for use with many cell types.

As an important feature for use with live cells, the MBBs and the overhangs attached to the structure exhibited stability for at least 24 h in the experimental cell culture conditions (Figure S2 and S3, Supporting Information), suggesting both mechanical function (e.g., shape, orientation, stiffness) and chemical function (e.g., sequence-specific binding) programed into the structure are stable over 24 h. The extended stability may be due to the close-packed nature of dsDNA helices in a multilayer DNA origami design like the MBB, which could make them less susceptible to enzymatic degradation. We observed a slight decrease of MBBs attached on the cell surface over the timescale of 1 h (Figure 3C). A fraction of MBB structures were internalized over timescale of  $\approx 1$  h (Figure S7, Supporting Information), which is consistent with prior studies that have demonstrated the uptake of DNA origami nanostructures from solution via endocytosis within several hours.<sup>[11]</sup> The level of MBB on the surface remained steady after 1 h with approximately half of the structures still remaining stably bound to the cell surface for at least 2 h (Figure S7, Supporting Information).

Interestingly, some cell types exhibited increased levels of MBB binding to the surface. HPFs displayed the largest level of binding while HL-60s the smallest (Figure 2C). This variation in binding may be due to differences in the molecular composition of the cell membranes. For example, cholesterol and sphingolipid content within the membrane is known to vary widely among different cell types,<sup>[33]</sup> which could impact the incorporation of cholesterol-conjugated oligos. Some cells exhibited inhomogeneous distributions around the cell periphery (Figure 2C), which could be a result of the cholesterol-anchored MBBs localizing to cholesterol- and sphingolipid-enriched regions of the plasma membrane. Future work is required to fully understand DNA nanostructure localization in the cell surface, and this presents an exciting prospect of exploiting inherent mechanisms of self-assembly within cell membranes to localize and probe specific areas or components of the cell membrane.

We further demonstrated programmable control over DNA origami nanostructures on the cell surface using DNA strand displacement<sup>[29]</sup> as a method for detachment and demonstrating docking of additional DNA origami structures (Figure 3) establishing the cell membrane as a functional platform for the formation of hierarchical DNA assemblies. We leveraged our cell membrane functionalization and programmable higher order assembly of DNA origami nanostructures to facilitate mechanically stable adhesion between homotypic and heterotypic cells in a controllable manner using DNA origami nanostructures as cellular Velcro (CellCro) (Figure 4). This application of the MBB establishes a foundation to extend DNA nanotechnology

to program the formation of cell clusters and microtissues with controlled spatial heterogeneity.

Although prior work has utilized DNA strands bound to cell membranes to mediate target sensing<sup>[6]</sup> or cell–cell binding,<sup>[4]</sup> implementing DNA origami structures at the cell surfaces provides a distinct advantage for multiplexing function. The ability to specify device shape enables programming functional sites in controlled arrangement and orientation. In the future, these membrane-bound DNA origami structures could enable functional assembly within the membrane to mimic functional biomolecular complexes such as an immune synapse, especially given the wide use of DNA origami to template or organize proteins.<sup>[34]</sup> Moreover, given the rapidly growing scope of DNA nanotechnology, our MBB will enable the capability to implement numerous DNA device functions such as measurement of molecular forces,<sup>[17]</sup> programed motion and conformational changes,<sup>[30]</sup> sensing of extracellular target molecules,<sup>[13]</sup> intracellular pH measurements,<sup>[35]</sup> and local delivery of molecular payloads<sup>[10]</sup> at the surface of cells in their complex local environments. The characteristics of the MBB presented here, including the size and overhang binding specificity, could also allow for localization of many measurement functionalities on the same or distinct platforms on individual cells or imparting specific functions to certain cell types within mixed cell populations in lab-on-a-chip environments. More broadly, this work establishes a foundation to use DNA origami nanodevices as membrane engineering tools that can mimic and direct complex biological processes on the surface of various cell types in microtissue scale.

## Experimental Section

**Design, Fabrication, Purification, and Stability:** The MBB was designed using the software caDNAno<sup>[36]</sup> and fabricated using protocols developed by Castro et al.<sup>[37]</sup> Briefly, folding reactions containing 20 mM scaffold, 10-fold molar excess of staples (each staple at 200 mM) in a folding buffer (FOB) solution (5 mM Tris, 5 mM NaCl, 1 mM EDTA) with 20 mM MgCl<sub>2</sub> were subjected to thermal annealing by rapid heating to 65 °C followed by slow cooling to 4 °C over 2.5 d. Folding reactions were purified by centrifugation using a protocol slightly modified from ref. [38] (details in the Supporting Information). Purified structures were resuspended in FOB with 20 mM MgCl<sub>2</sub> and fluorescent oligonucleotides were added at 5 $\times$  excess with respect to the number of designated binding sites and incubated for at least 30 min. To remove the excess fluorescent oligonucleotides, the poly(ethylene glycol) (PEG) centrifugal purification procedure was repeated twice. To confirm MBB structural integrity and stability of overhangs under cell culture conditions, structures were resuspended in cell culture media supplemented with various levels of serum and MgCl<sub>2</sub> following PEG purification, and incubated for either 3 or 24 h at 37 °C. Agarose gel electrophoresis assay<sup>[37]</sup> followed by visualization of the excised gel bands on TEM<sup>[37]</sup> was used to address the stability of MBB under cell culture condition.

**MBB Cell Surface Incorporation:** Prior to resuspension in each experimental media condition, the cells were washed twice with 1 $\times$  phosphate buffered saline (PBS) without MgCl<sub>2</sub>/CaCl<sub>2</sub>. The washed cells were then resuspended in the experimental media at 5000 cells  $\mu\text{L}^{-1}$  for incubation with 10 mM MIO for 5 min at 37 °C. The cells were then washed once in the experimental medium to remove the extra MIO. The 60-base bridge oligo was added at 1 mM for 5 min at 37 °C followed by the addition of the 20-base pair fortifier oligos at 1 mM for another 5 min at 37 °C. To remove the excess bridge and fortifier oligos, the incubated cells were washed once with the experimental medium.

Finally, the nanostructures were added at 5 mM for 5 min at 37 °C. Cells were washed a final time to remove excess nanostructures and the final sample was transferred to an 8-well imaging dish. Additional details for different cell types, experimental media conditions, and fluorescence imaging are provided in the Supporting Information.

**The Detachment of MBB Bound to CH12.LX Plasma Membrane:** The CH12.LX cells were functionalized with MBB as previously described. The fortifier oligos were excluded to provide a toehold for the binding of detachment oligos. Cells functionalized with MBB at 1500 cells  $\mu\text{L}^{-1}$  were split into two main samples with and without the addition of 1 mM detachment oligo. The samples were incubated at 37 °C and samples of cells were taken out at varying time points to monitor the MBB attachment to the cell membrane.

**The Vertical Assembly of Secondary Nanoplatfoms:** The dMBBs that feature six binding overhangs on the outward-facing side were preincubated with 1 mM of the 45-base COs for 5 min at 37 °C and used to functionalize the surface of CH12.LX cells using the previously described method. The cells functionalized with dMBBs that featured the COs were then incubated with sMBB to vertically assemble the nanostructures on the surface of the cell. Fluorescent microscopy was used to visualize both the dMBB labeled with Alexa 647 oligos and the sMBB labeled with Alexa 488 oligos. To confirm the specificity of the stacking technique, the case without the COs was used as a control.

**Controllable Cell–Cell Adhesion:** The dMBBs were preincubated with excess CO prior to cell surface binding. Both dMBB and sMBB were incorporated into the membrane of two separate subpopulations of cells as previously described. The two subpopulations were then mixed for imaging. Prior to introducing cells, the imaging chamber surface was treated with casein at 0.1 mg  $\text{mL}^{-1}$  casein for 30 min at 37 °C. This resulted in the condition where some cells were adhered to the surface and some were floating. An Optical Trap was used to guide floating cells featuring either dMBB or sMBB toward an anchored cell with complementary MBB on the surface. The pair of cells were kept in contact for 1 min, then the optical trap was used to steer the free cell away from the stationary cell, generating tension between the two cells. The stability of attachment between the pair of cells under tension was monitored and compared to the control case in the absence of the CO.

**Statistical Analysis:** One-way ANOVA test was used to ensure statistical significance in Figure 2C. Two-sided student t-test was used to report the statistical significance of the fold change data in Figure 2C, 3C,F, and 4C,E. Equal variance assumption was used between each pair of data pools. The statistical toolbox provided by MATLAB was used to report the *p*-values. Levels of significance were reported as follows: \*, *p* < 0.05; \*\*\*, *p* < 0.001.

## Supporting Information

Supporting Information is available from the Wiley Online Library or from the author.

## Acknowledgements

E.A. and M.Y.M. contributed equally to this work. This work was supported by grants from the National Science Foundation (Award no. 1351159 to CEC) and the American Heart Association (Award no. 15SDG25480000 to JWS and no. 17IRG33460357 to CEC). In addition, the work was partially supported by The Ohio State University Materials Research Seed Grant Program, funded by the Center for Emergent Materials, an NSF-MRSEC, grant DMR-1420451, the Center for Exploration of Novel Complex Materials, and the Institute for Materials Research. C.R.L. is a recipient of a National Institutes of Health T32 Award in Oncology Training Fellowship at The Ohio State University Comprehensive Cancer Center, T32 CA009338. The authors also thank Emily McKinnon for the preliminary design of the DNA origami structure.

## Conflict of Interest

The authors declare no conflict of interest.

## Keywords

cell surface engineering, DNA nanotechnology, DNA origami, intercellular adhesion, membrane functionalization

Received: June 29, 2017

Revised: August 8, 2017

Published online: October 13, 2017

- [1] a) R. M. Gordley, L. J. Bugaj, W. A. Lim, *Curr. Opin. Struct. Biol.* **2016**, *39*, 106; b) A. Levsikaya, O. D. Weiner, W. A. Lim, C. A. Voigt, *Nature* **2009**, *461*, 997; c) L. Morsut, K. T. Roybal, X. Xiong, R. M. Gordley, S. M. Coyle, M. Thomson, W. A. Lim, *Cell* **2016**, *164*, 780.
- [2] a) Q. Li, C. R. So, A. Fegan, V. Cody, M. Sarikaya, D. A. Vallera, C. R. Wagner, *J. Am. Chem. Soc.* **2010**, *132*, 17247; b) K. Gabrielse, A. Gangar, N. Kumar, J. C. Lee, A. Fegan, J. J. Shen, Q. Li, D. Vallera, C. R. Wagner, *Angew. Chem., Int. Ed. Engl.* **2014**, *53*, 5112.
- [3] Z. J. Gartner, C. R. Bertozzi, *Proc. Nat. Acad. Sci.* **2009**, *106*, 4606.
- [4] M. E. Todhunter, N. Y. Jee, A. J. Hughes, M. C. Coyle, A. Cerchiari, J. Farlow, J. C. Garbe, M. A. LaBarge, T. A. Desai, Z. J. Gartner, *Nat. Methods* **2015**, *12*, 975.
- [5] T. Tokunaga, S. Namiki, K. Yamada, T. Imaishi, H. Nonaka, K. Hirose, S. Sando, *J. Am. Chem. Soc.* **2012**, *134*, 9561.
- [6] W. Zhao, S. Schafer, J. Choi, Y. J. Yamanaka, M. L. Lombardi, S. Bose, A. L. Carlson, J. A. Phillips, W. Teo, I. A. Droujinine, *Nat. Nanotechnol.* **2011**, *6*, 524.
- [7] J. R. Burns, N. Al-Juffali, S. M. Janes, S. Howorka, *Angew. Chem., Int. Ed.* **2014**, *53*, 12466.
- [8] N. C. Seeman, *J. Theor. Biol.* **1982**, *99*, 237.
- [9] a) P. W. Rothmund, *Nature* **2006**, *440*, 297; b) C. J. Kearney, C. R. Lucas, F. J. O'Brien, C. E. Castro, *Adv. Mater.* **2016**, *28*, 5509.
- [10] S. M. Douglas, I. Bachelet, G. M. Church, *Science* **2012**, *335*, 831.
- [11] P. D. Halley, C. R. Lucas, E. M. McWilliams, M. J. Webber, R. A. Patton, C. Kural, D. M. Lucas, J. C. Byrd, C. E. Castro, *Small* **2016**, *12*, 308.
- [12] Q. Zhang, Q. Jiang, N. Li, L. Dai, Q. Liu, L. Song, J. Wang, Y. Li, J. Tian, B. Ding, Y. Du, *ACS Nano* **2014**, *8*, 6633.
- [13] D. Wang, Y. Fu, J. Yan, B. Zhao, B. Dai, J. Chao, H. Liu, D. He, Y. Zhang, C. Fan, *Anal. Chem.* **2014**, *86*, 1932.
- [14] D. Koirala, P. Shrestha, T. Emura, K. Hidaka, S. Mandal, M. Endo, H. Sugiyama, H. Mao, *Angew. Chem., Int. Ed. Engl.* **2014**, *53*, 8137.
- [15] J. J. Funke, H. Dietz, *Nat. Nanotech.* **2016**, *11*, 47.
- [16] a) J. V. Le, Y. Luo, M. A. Darcy, C. R. Lucas, M. F. Goodwin, M. G. Poirier, C. E. Castro, *ACS Nano* **2016**, *10*, 7073; b) J. J. Funke, P. Ketterer, C. Lieleg, S. Schunter, P. Korber, H. Dietz, *Sci. Adv.* **2016**, *2*, e1600974; c) F. Kilchherr, C. Wachauf, B. Pelz, M. Rief, M. Zacharias, H. Dietz, *Science* **2016**, *353*, aaf5508.
- [17] P. C. Nickels, B. Wünsch, P. Holzmeister, W. Bae, L. M. Kneer, D. Grohmann, P. Tinnefeld, T. Liedl, *Science* **2016**, *354*, 305.
- [18] M. Langecker, V. Arnaut, J. List, F. C. Simmel, *Acc. Chem. Res.* **2014**, *47*, 1807.
- [19] M. Langecker, V. Arnaut, T. G. Martin, J. List, S. Renner, M. Mayer, H. Dietz, F. C. Simmel, *Science* **2012**, *338*, 932.
- [20] J. R. Burns, A. Seifert, N. Fertig, S. Howorka, *Nat. Nanotechnol.* **2016**, *11*, 152.
- [21] A. Johnson-Buck, S. Jiang, H. Yan, N. G. Walter, *ACS Nano* **2014**, *8*, 5641.



- [22] A. Czogalla, D. J. Kauert, R. Seidel, P. Schwille, E. P. Petrov, *Nano Lett.* **2014**, *15*, 649.
- [23] a) Y. Suzuki, M. Endo, Y. Yang, H. Sugiyama, *J. Am. Chem. Soc.* **2014**, *136*, 1714; b) S. Kocabey, S. Kempter, J. List, Y. Xing, W. Bae, D. Schifffels, W. M. Shih, F. C. Simmel, T. Liedl, *ACS Nano* **2015**, *9*, 3530.
- [24] Y. Yang, J. Wang, H. Shigematsu, W. Xu, W. M. Shih, J. E. Rothman, C. Lin, *Nat. Chem.* **2016**, *8*, 476.
- [25] a) R. O. Pedersen, E. G. Lobo, T. H. LaBean, *Biomacromolecules* **2013**, *14*, 4157; b) A. Shaw, V. Lundin, E. Petrova, F. Fördös, E. Benson, A. Al-Amin, A. Herland, A. Blokzijl, B. Högberg, A. I. Teixeira, *Nat. Methods* **2014**, *11*, 841.
- [26] S. M. Douglas, H. Dietz, T. Liedl, B. Högberg, F. Graf, W. M. Shih, *Nature* **2009**, *459*, 414.
- [27] J. Hahn, S. F. Wickham, W. M. Shih, S. D. Perrault, *ACS Nano* **2014**, *8*, 8765.
- [28] R. Veneziano, S. Ratanalert, K. Zhang, F. Zhang, H. Yan, W. Chiu, M. Bathe, *Science* **2016**, *352*, 1534.
- [29] B. Yurke, A. J. Turberfield, A. P. Mills, F. C. Simmel, J. L. Neumann, *Nature* **2000**, *406*, 605.
- [30] A. E. Marras, L. Zhou, H.-J. Su, C. E. Castro, *Proc. Nat. Acad. Sci.* **2015**, *112*, 713.
- [31] D. Y. Zhang, G. Seelig, *Nat. Chem.* **2011**, *3*, 103.
- [32] J. List, M. Weber, F. C. Simmel, *Angew. Chem., Int. Ed.* **2014**, *53*, 4236.
- [33] I. Levental, S. L. Veatch, *J. Mol. Biol.* **2016**, *428*, 4749.
- [34] a) B. Sacca, R. Meyer, M. Erkelenz, K. Kiko, A. Arndt, H. Schroeder, K. S. Rabe, C. M. Niemeyer, *Angew. Chem., Int. Ed. Engl.* **2010**, *49*, 9378; b) W. Xu, B. Nathwani, C. Lin, J. Wang, E. Karatekin, F. Pincet, W. Shih, J. E. Rothman, *J. Am. Chem. Soc.* **2016**, *138*, 4439.
- [35] S. Modi, C. Nizak, S. Surana, S. Halder, Y. Krishnan, *Nat. Nanotechnol.* **2013**, *8*, 459.
- [36] S. M. Douglas, A. H. Marblestone, S. Teerapittayanon, A. Vazquez, G. M. Church, W. M. Shih, *Nucleic Acids Res.* **2009**, *37*, gkp436.
- [37] C. E. Castro, F. Kilchherr, D.-N. Kim, E. L. Shiao, T. Wauer, P. Wortmann, M. Bathe, H. Dietz, *Nat. Methods* **2011**, *8*, 221.
- [38] E. Stahl, T. G. Martin, F. Praetorius, H. Dietz, *Angew. Chem.* **2014**, *126*, 12949.
- [39] G. Houghton, L. W. Arnold, G. A. Bishop, T. J. Mercolino, *Immunol. Rev.* **1986**, *93*, 35.
- [40] a) R. Gallagher, S. Collins, J. Trujillo, K. McCredie, M. Ahearn, S. Tsai, R. Metzgar, G. Aulakh, R. Ting, F. Ruscetti, *Blood* **1979**, *54*, 713; b) S. J. Collins, R. C. Gallo, R. E. Gallagher, *Nature* **1977**, *270*, 347.
- [41] J. Debnath, S. K. Muthuswamy, J. S. Brugge, *Methods* **2003**, *30*, 256.
- [42] K. C. Neuman, S. M. Block, *Rev. Sci. Instrum.* **2004**, *75*, 2787.